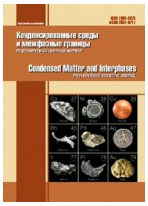

ISSN 1606-867X (Print)
ISSN 2687-0711 (Online)
Condensed Matter and Interphases
Kondensirovannye Sredy i Mezhfaznye Granitsy
https://journals.vsu.ru/kcmf/

Articles of issue 1

Original articles

Research article
https://doi.org/10.17308/kcmf.2025.27/12624

Analysis of the crystalline quality of bulk $In_{0.83}Ga(Al)_{0.17}$ layers formed on metamorphic InAlAs/InP buffer layers with linear and nonlinearcomposition gradients

E. I. Vasilkova[1,2]✉, E. V. Pirogov[1], V. N. Nevedomsky[3], O. V. Barantsev[1], K. O. Voropaev[4], A. A. Vasiliev[4], L. Ya. Karachinsky[1,5], I. I. Novikov[1,5], M. S. Sobolev[1,2,5]

[1]*Alferov University,*
8/3 Khlopina st., Saint Petersburg 194021, Russian Federation

[2]*St. Petersburg Electrotechnical University "LETI",*
5 Professora Popova ul., Saint Petersburg 197022, Russian Federation

[3]*Ioffe Institute,*
26 Politekhnicheskaya st., Saint Petersburg 194021, Russian Federation

[4]*JSC "OKB-Planeta",*
13a, room 1n Bolshaya Moskovskaya st., Velikiy Novgorod 173004, Russian Federation

[5]*LLC "Connector Optics",*
16 litera B Domostroitelnaya ul., Saint Petersburg 194292, Russian Federation

Abstract

This paper investigates the effectiveness of metamorphic InAlAs buffer layers with linear and root-like dependence of the In mole fraction in the composition for the growth of bulk $In_{0.83}Ga(Al)_{0.17}As$ layers on InP substrates. The analysis of the X-ray diffraction reciprocal space maps showed that in both cases $In_{0.83}Ga(Al)_{0.17}As$ layers were partially strain-free. One of the mechanisms of strain relaxation during the growth of the linearly graded buffer layer is the rotation of the crystal lattice, while the mechanism of strain relaxation during the growth of the convex-graded buffer layer is a 0.82° tilt of the crystal lattice without any rotation. According to the images obtained by transmission electron microscopy, the density of threading dislocations in the upper InGaAs layers grown on the buffer layer with a linear composition gradient is ~ $5 \cdot 10^8$ cm^{-2}.

Keywords: Metamorphic buffer layers, Reciprocal space mapping of X-ray diffraction intensity, Transmission electron microscopy, Molecular beam epitaxy

Funding: The study was funded by the Russian Science Foundation, research project No. 22-79-00146.

For citation: Vasilkova E. I., Pirogov E. V., Nevedomsky V. N., Barantsev O. V., Voropaev K. O., Vasiliev A. A., Karachinsky L. Ya., Novikov I. I., Sobolev M. S. Analysis of the crystalline quality of bulk $In_{0.83}Ga(Al)_{0.17}As$ layers formed on metamorphic InAlAs/InP buffer layers with linear and nonlinearcomposition gradients. *Condensed Matter and Interphases*. 2025;27(1): 86–95. https://doi.org/10.17308/kcmf.2025.27/12624

Для цитирования: Василькова Е. И., Пирогов Е. В., Неведомский В. Н., Баранцев О. В., Воропаев К. О., Васильев А. А., Карачинский Л. Я., Новиков И. И., Соболев М. С. Анализ кристаллического качества объемных слоев $In_{0.83}Ga(Al)_{0.17}As$, сформированных на метаморфных буферных слоях InAlAs/InP с линейным и нелинейным градиентом состава. *Конденсированные среды и межфазные границы*. 2025;27(1): 86–950. https://doi.org/10.17308/kcmf.2025.27/12624

✉ Elena I. Vasilkova, e-mail: elenvasilkov@gmail.com

1. Introduction

The possibility of growing semiconductor layers on lattice-mismatched substrates has become an important factor contributing to the rapid development of epitaxial technologies. This achievement has allowed observing new electrophysical and optical effects in heterostructures and has considerably expanded the range of components for heterostructural nano- and optoelectronics. One of the traditional epitaxy-based approaches to obtaining semiconductor layers on substrates with a critically large mismatch in the crystal lattice parameters is the metamorphic growth. Metamorphic buffer layers (MBL) create a transition from the substrate lattice constant to the lattice constant required for the growth of the functional layers of the heterostructure. One way to enable such a transition is to gradually change the composition of the buffer layer, which means changing material fluxes during the MBL epitaxial growth. The change of the composition can be either smooth, for example, when a linear dependence is involved, or step-like. Typically, the thickness of the MBLs is a few micrometers. The MBL formation must result in a planar epitaxial surface for the subsequent strain-free growth of the active layers. The MBL technology is currently widely used for the manufacture of transistors with high mobility of electrons, lasers, solar cells, photodiodes, etc. [1–6]. Various designs, thicknesses, and materials of buffer layers are studied and applied depending on the active layers of the heterostructure and its application in devices.

This paper is devoted to the study of possible designs of a metamorphic buffer layer for the growth of $In_{0.83}Ga_{0.17}As$ triple solid solutions on InP substrates. These two materials are used for the manufacture of near-infrared spectral photodetectors, in which the peak wavelength of the photoresponse depends on the indium content in the photo-absorbing layer of InGaAs. The most common option is an absorbing layer of a $In_{0.53}Ga_{0.47}As$ solid solution, which is lattice-matched with InP. The high quality of InP substrates, as well as the excellent characteristics of photodiodes and matrix photodetectors based on $In_{0.53}Ga_{0.47}As$/InP, allowed InGaAs to become the leading material for the manufacture of photodetectors operating in the wavelength of 1–1.7 μm. With an increase in the indium content to the mole fraction of x = 0.83, the detection range shifts to a longer wavelength region of 2.2–2.6 μm. Thus, by varying the composition of the absorbing layer, a wider near-infrared region of the spectrum can be covered within the same system of materials. However, due to a large relative mismatch between the lattice parameters of $In_{0.83}Ga_{0.17}As$ and the InP substrate of ~ 2%, the critical thickness for the pseudomorphic growth of the active layer is 1-2 orders of magnitude less than the thickness required for the effective absorption of the emission [7]. Therefore, in order to avoid the appearance of a large number of misfit dislocations in the active region during the growth of the $In_{0.83}Ga_{0.17}As$ layer on the surface of InP, it is necessary to grow transitional metamorphic buffer layers. In this case, MBLs contribute to the pseudomorphic growth of the InGaAs absorbing layers and, consequently, reduce the density of the resulting misfit dislocations, and also stop the penetration of threading dislocations into the active layers of the photodetectors. Dislocations have adverse effects on photodetectors since they contribute to some mechanisms of dark current formation, which leads to a reduced detectivity of devices [8].

2. Experimental

The research involved growing experimental samples containing MBLs of various designs by means of molecular-beam epitaxy using a Riber MBE49 unit (Fig. 1). The samples were InAlAs/InGaAs heterostructures on n^+-InP (100) "epi-ready" doped substrates. The heterostructures included a ~ 0.1 μm thick layer of $In_{0.52}Al_{0.48}As$ which was lattice-matched with the substrate, InAlAs MBLs of ~ 2 μm of various configurations, an active region of $In_{0.83}Ga_{0.17}As$ with a thickness of ~ 1.5 μm, and upper contact layers of $In_{0.83}Al(Ga)_{0.17}As$ with a thickness of ~ 650 nm (Fig. 1). The MBLs were grown at a constant temperature of the substrate, which was 70 °C lower than the growth temperature of the active region (490 °C). The process was concluded with a thermal cycling: the peak temperature rose to 530 °C followed by cooling to 100 °C. The buffer layers were doped with silicon to a level of $1 \cdot 10^{18}$ cm^{-3} (n^+), while the contact layers were doped with

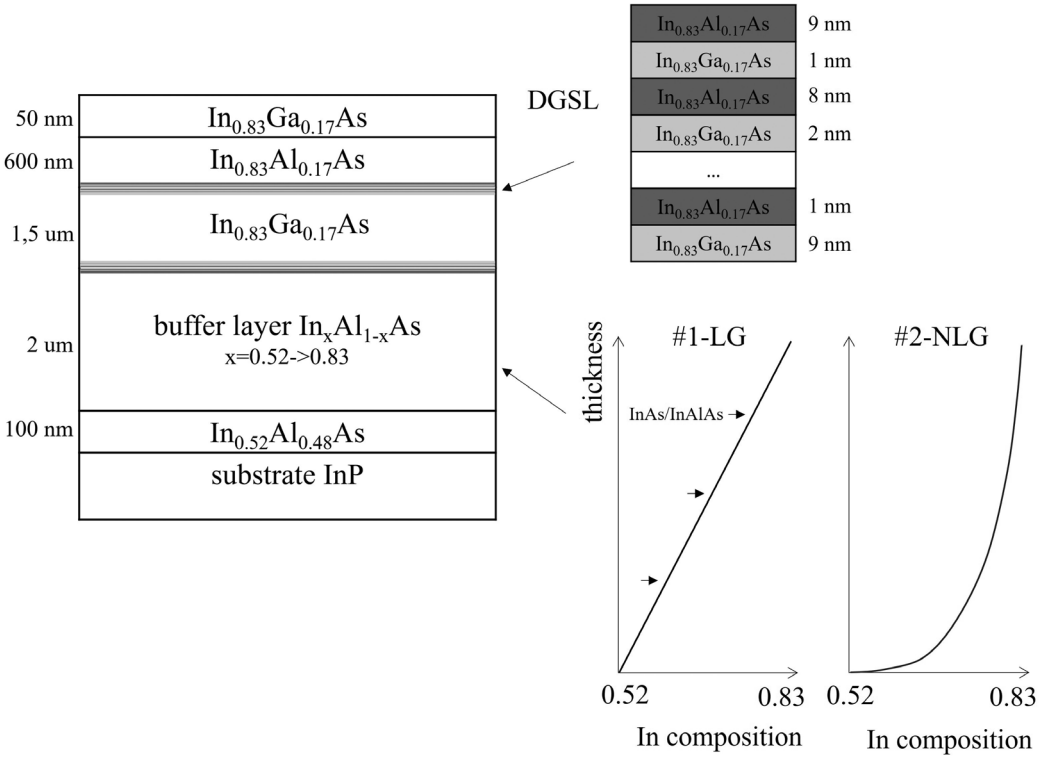

Fig. 1. Schematic image representing the layer composition of metamorphic heterostructures #1-LG и #2-NLG

beryllium, with an impurity concentration of $2 \cdot 10^{18}$ cm^{-3} (p^+). The active region of InGaAs was also doped with silicon at a low concentration of $2 \cdot 10^{16}$ cm^{-3}. The type and concentration of the dopant in each layer were selected in order to obtain a diode heterostructure for the subsequent manufacture of PIN photodiode crystals with an absorbing layer of $In_{0.83}Ga_{0.17}As$.

Sample 1-LG contained $In_xAl_{1-x}As$ MBLs with a linear gradient of indium composition from x = 0.52 to x = 0.83 and with intermediate inserts of three InAs(4 Å)/InAlAs(10 Å) periods every 500 nm. Buffer layers of a similar design showed an advantage over the stepwise changing of the composition and the linear changing of the composition without inserts [9]. The demonstrated benefit of using this type of MBLs was in the lower density of threading dislocations in the functional layers and the existence of a dislocation-free region d_{free} in the buffer layer.

The buffer layer of the 2-NLG sample was the $In_xAl_{1-x}As$ layer whose composition changed following the nonlinear convex gradient which approximated the square root-like dependence. The fraction of InAs in the composition also varied from 0.52 to 0.83. The main difference between the 1-LG and 2-NLG samples was that when the convex gradient of the composition was applied, the MBL crystal lattice parameter grew faster in its lower region bordering the substrate, and, conversely, more smoothly when approaching the active layers. Therefore, it can be assumed that dislocations formed more actively in the lower part of the MBLs, which was most distant from the functional layers of the heterostructure. Previous studies used metamorphic InAlAs layers on GaAs substrates to demonstrate the advantages of such a design as compared to a linear profile in terms of more effective elastic strain relaxation [10]. Also, using the example of the InAlAs/GaAs system of materials, it was experimentally confirmed that the root-like dependence of the indium composition in MBLs resulted in a lower density of dislocations and the formation of a thicker d_{free} region [11].

To reduce the conduction band discontinuity between InGaAs and InAlAs and the dislocation density, the so-called digital-graded superlattices (DGSL) were introduced into the structure of the heterostructures from above and below the absorbing layer, which consisted of 9-period $In_{0.83}Ga_{0.17}As/In_{0.83}Al_{0.17}As$ superlattices with a

total thickness of about 90 nm [12]. The well-to-barrier ratio in the DGSL period ranged from 1:9 to 9:1 in the case of the lower superlattice (MBL-active region heterointerface) and was mirrored in the case of the upper superlattice (active region-contact layer heterointerface). These superlattices created a stepped barrier for charge carriers at the point of conduction band discontinuity in the heterostructure. What is more, the additional heterointerfaces that DGSLs created were expected to facilitate a smoother transition from the lattice constant of InGaAs to InAlAs if there was any residual strain in InGaAs. Therefore, DGSL regions were inserted in both samples before the growth of the $In_{0.83}Ga_{0.17}As$ absorbing layer and after its complete formation.

The main experiments aimed at studying the crystalline properties of the samples of metamorphic heterostructures were preceded by their electrochemical capacitance–voltage (ECV) measurements. A comparison of the profiles of the distribution of the charge carriers concentration in the 1-LG and 2-NLG samples along the depth of the structure is shown in Fig. 2. The profile of the 1-LG sample was smoother and more comparable to the structure of the heterostructure in terms of layer thickness. It also did not have spikes and abrupt changes in concentration, unlike the 2-NLG sample. This may be evidence of a higher defectiveness of the 2-NLG sample with the root profile of the buffer layer composition. Based on the obtained results of the ECV measurements, the 1-LG sample with a linear MBL was selected as a reference for the study by the destructive transmission electron microscopy (TEM). In addition, X-ray reflection spectra were measured for both samples, and reciprocal space maps of X-ray diffraction intensity were constructed and analyzed.

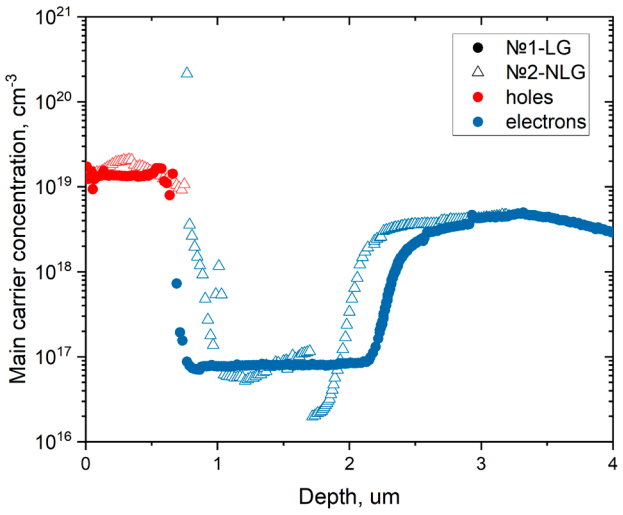

Fig. 2. Main carrier concentration profiles, obtained by electrochemical capacitance-voltage profiling

3. Results and discussion

3.1. Transmission electron microscopy

The 1-LG sample was examined by SEM in the cross-section geometry (110) on a JEM2100F (Jeol) electron microscope at an accelerating voltage of 200 kV. A standard method was used to prepare the sample, which involved thinning by precision grinding and spraying with argon ions during the final stage prior to perforation.

The obtained TEM image (Fig. 3) allowed identifying the regions of the MBLs, the InGaAs absorbing layer, and the InAl(Ga)As contact layers. In the image, the InP substrate is at the bottom and is separated from the metamorphic heterostructure by a bright white band. In the MBL, there was a large number of misfit dislocations in the form of horizontal dark bands and threading dislocations in the form of inclined dark lines. The dislocations were evenly distributed over the thickness of the MBL, and a rough estimate of the density of the extended defects in the buffer layer was ~ $1 \cdot 10^{11}$ cm^{-2}. Fig. 3

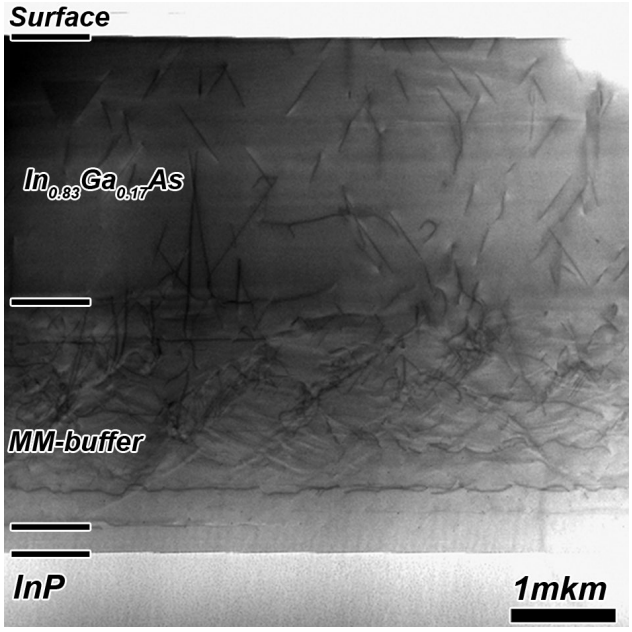

Fig. 3. STEM image of sample #1-LG

shows that some dislocations were directly under the heterointerfaces of the InAs/InAlAs inserts, especially during the initial stages of the MBL growth. Also, threading dislocations were bending on various heterointerfaces, including in the DGSL region, however, their complete bending and annihilation occurred less often.

Earlier studies of test MBL heterostructures with a linear composition gradient revealed the existence of a dislocation-free region d_{free} [9]. Based on current images, it was impossible to judge whether the d_{free} region was present. What is more, the density of defects in the sample was much higher than the density of defects in the test MBL structure. Thus, according to the TEM images in the cross-sectional geometry, the density of the threading dislocations revealed in the functional layers of the $In_{0.83}Al_{0.17}As$ and $In_{0.83}Ga_{0.17}As$ heterostructures was ~ $5 \cdot 10^8$ cm^{-2}, while in the test structure, the density of dislocations in the $In_{0.83}Ga_{0.17}As$ layer with a thickness of 500 nm was below the detection limit of the method, i.e. < $1 \cdot 10^6$ cm^{-2} [9]. Perhaps this was due to the absence of the inverse step in the InAlAs composition gradient, which was introduced into the MBL design of the test structure. The absence of the inverse step could also affect the density of threading dislocations in the InGaAs absorbing layer.

3.2. X-ray diffractometry and reciprocal space mapping of X-ray diffraction intensity

Information about the presence of elastic strain, misfit dislocations, and crystal lattice disorientation can be obtained from the X-ray diffraction reciprocal space mapping [13]. The X-ray diffraction reciprocal space map is a projection of the three-dimensional intensity distribution of the X-ray reflection intensity from the sample on the orthogonal axes of the reciprocal space qX <110> and qZ [001] which are parallel to the surfaces of the heterostructure and orthogonal to the surface of the heterostructure, respectively. The reciprocal space map is a set of contours of equal intensity, the greatest contribution to which is made by diffraction reflections from the selected family of crystalline planes. The X-ray scattering was recorded in the angular coordinates ω-2θ, which were then converted into the reduced coordinates of the reciprocal space qX and qZ. X-ray diffraction spectra were recorded on a DRON-8 X-ray diffractometer (Burevestnik, Russia) with a Bartels monochromator and the radiation at the X-ray tube of Cu$K\alpha 1$ = 0.15406 nm. The maps were converted and processed with the accompanying software package Reciprocal Space Mapping by *Burevestnik*.

Reciprocal space maps of X-ray diffraction intensity for reflections (224) for the samples were constructed and analyzed (Fig. 4). The reciprocal space mapping of X-ray diffraction intensity in the case of asymmetric reflection, for example, from a set of planes (224), allowed making judgements about the residual strain in the epitaxial layers. In Figures 4a and 4b, broad maxima of high intensity characterize diffraction on the functional layers of $In_{0.83}Al_{0.17}As/In_{0.83}Ga_{0.17}As$ of the 1-LG and 2-NLG samples, respectively. Lines drawn in the images in Fig. 4 characterize an entirely strain-free (solid line) and entirely pseudomorphic (dashed line) state of the crystal in relation to the substrate [14]. The line of the entire stain relaxation for reflection (224) always passes through the peak of the substrate, therefore, the position of the InGaAlAs maximum relative to this line can be used to conclude about the degree of strain relaxation in this layer. In both studied samples, the lines of strain relaxation passed near the reflection from the InGaAlAs layers, however, they did not cross its maximum. Thus, the active layers in both 1-LG sample and 2-NLG sample were partially strain-free.

The measurements of symmetric (004) reflections of the samples allowed making conclusions about the imperfection of the crystal lattice of the grown layers since the broadening of the intensity contours along the qX direction indicated dislocations or a mosaic structure, while the broadening along the qZ direction meant there was a fluctuation of the perpendicular component of the lattice parameter [15]. Let us assume that direction [110] of the X-ray beam incidence along the base cut of the substrate is an azimuthal angle of 0°, while direction [1$\underline{1}$0], which is perpendicular to the base cut is an azimuth of 90°. X-ray scattering patterns from a set of reflecting planes (004) of the 1-LG and 2-NLG samples in the reciprocal space are shown in Fig. 5. The narrower and more intense

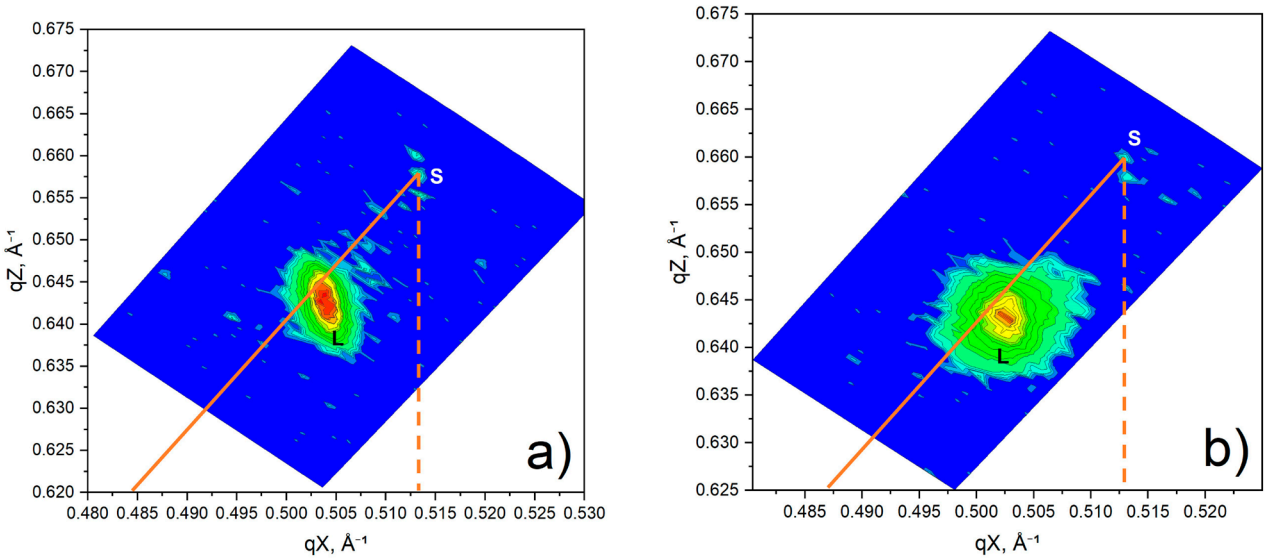

Fig. 4. Reciprocal space maps of asymmetric (224) reflection: a) sample #1-LG, б) sample #2-NLG. Labels S and L stand for reflection peaks from InP substrate and $In_{0.83}Ga(Al)_{0.17}As$ active layers. Orange lines represent fully relaxed (solid) and pseudomorphic (dashed) states

maximum at the top of all images corresponds to the InP substrate and is comparable to the angular coordinate 2θ = 63.34°.

Let us consider Fig. 5a for a symmetrical reflection of the 1-LG sample with an azimuthal angle of 0° corresponding to the *qX* direction [110]. A continuous green region of medium intensity, elongated along the *qZ* axis, is characteristic of MBLs with a smooth composition gradient. The experimental maximum of the functional layers of $In_{0.83}Al_{0.17}As/In_{0.83}Ga_{0.17}As$ (individual maxima of each layer are difficult to distinguish due to very close values of the lattice constant), located lower along the *qZ* axis, is shifted along the *qX* axis relative to the maximum of the substrate, and, as compared to it, has a more pronounced ellipticity. The coordinate of the $In_{0.83}Ga(Al)_{0.17}As$ peak along the *qZ* axis corresponds to an angle of 2θ = 61.79°. This peak, as compared to the peak of the substrate, is much more stretched along both axes and its width in the *qX* direction exceeds many times the spread along *qZ*. Thus, we can assume that active layers of this sample have more local strain-free regions than regions with an elastically deformed lattice [15].

In the scattering pattern of the 2-NLG sample with similar conditions depicted in Fig. 5c, the maxima of diffraction intensity on the substrate and on the active layer are at the same positions along the *qZ* axis. However, in the case of the 2-NLG sample, the reciprocal space mapping did not reveal any significant reflection continuously stretched from the gradient buffer layer along the *qZ* axis. In addition, unlike the 1-LG sample, the maximum of the InGaAs layer was on the *qX* = 0 line. What is more, it was elongated mainly along the *qZ* axis and was characterized by a much less expressed diffusion scattering along the *qX* axis than in Fig. 5a. As we noted above, the broadening of the peak along *qZ* may be due to a fluctuation of the lattice constant in a direction perpendicular to the scanning planes. Thus, a significant blurring of the maximum along the vertical axis may indicate the existence of local deformed regions of the crystal lattice and an inhomogeneous strain distribution over the crystal.

The half-width peaks of the intensity of the reflected X-ray emission along the ω axis in the angular coordinates of direct space ω-2θ characterizes the defectiveness of the structure, which in the metamorphic heterostructure is mainly contributed by misfit dislocations of the screw type. The assessment of the dependence of the half-width intensity peaks relative to the ω axis on the normal lattice parameter $c = 2\lambda/sin(\theta)$ [16] and the TEM images allowed characterizing the distribution of defects in the 1-LG sample. The results showed that the defectiveness of the linear MBL first increased with a thickness, was maximum in the middle and upper parts

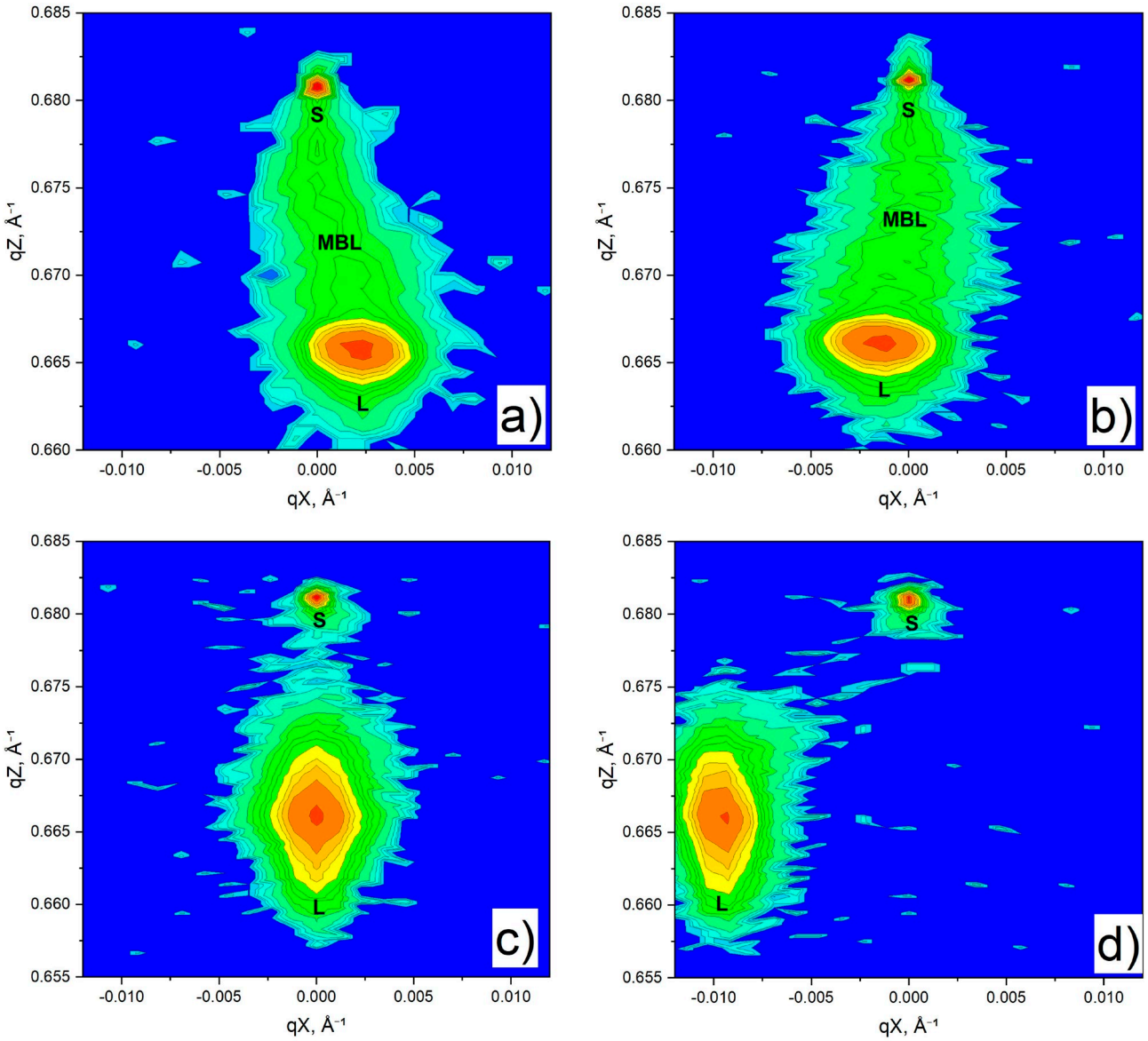

Fig. 5. Reciprocal space maps of symmetric (004) reflection of sample #1-LG (top) for azimuthal angles 0° (a) и 90° (b) and sample #2-NLG (bottom) for 0° (c) and 90° (d). Labels S, L and MBL stand for reflection peaks from InP substrate, $In_{0.83}Ga(Al)_{0.17}As$ active layers and $In_xAl_{1-x}As$ metamorphic buffer layer

of the buffer layer, and then decreased slightly just before the formation of the DGSL and the absorbing layer.

It should be noted that when rotating the 1-LG sample by an azimuthal angle of 90° (Fig. 5b), the maximum lateral coordinate of $In_{0.83}Ga(Al)_{0.17}As$ changed its sign relative to the $qX = 0$ axis, while the position of the peak along the qZ axis remained unchanged. However, similar to the case shown in Fig. 5a, the intensity spot from the linear MBL shifted uniformly towards the positive or negative qX, respectively. Fig. 5d shows images for the 2-NLG sample with an azimuthal angle of 90°. When rotating the sample with the root MBL by 90°, there was also a discrepancy between the maximum coordinates of the absorbing layer, however, in this case there was an abrupt change in the coordinate relative to $qX = 0$.

The mismatch between the maximum coordinates of the active layers and the substrate in the qX direction for the studied case of symmetrical reflection indicated the disorientation of the crystal lattice of the active layers relative to plane (001) [15]. The angle of the epitaxial layer disorientation relative to the substrate was characterized by inclination,

rotation, or torsion. In lattice-mismatched heterostructures on substrates with orientation (001), disorientation could occur due to uneven distribution of dislocations over the surface relative to directions [110] and [1$\underline{1}$0] [17]. This resulted in anisotropy of residual strain along these directions and could affect the angle of disorientation.

The reciprocal space mapping in the geometry of symmetrical reflections allowed estimating the inclination and rotation angles of the crystal lattice in the active layer relative to the plane of the substrate (001). For calculations, we used the relations given in [18, 19]:

$$\mathrm{tg}(\alpha_{0^\circ,90^\circ}) = \frac{\left|\Delta qX^{004}\right|_{0^\circ,90^\circ}}{4 / a_{sub} - \left|\Delta qZ^{004}\right|_{0^\circ,90^\circ}}$$

$$\mathrm{tg}(\varphi) = \alpha_{0^\circ} / \alpha_{90^\circ},$$

where α_{sub} = 5.8687 Å is the lattice constant of the substrate, qX^{004} is the difference in qX coordinates of the maxima of the layer and the substrate during symmetrical scanning (004), qZ^{004} is the difference in qZ coordinates of the maxima of the layer and the substrate during symmetrical scanning (004), α_{0° and α_{90° are the inclination angles of the crystal lattice at azimuthal angles of 0° and 90°, and φ is the azimuth of the zero inclination of the layer.

From Figures 5a and 5b, according to the given formulas, we obtained the inclination angles: α_{0° = 0.19°, α_{90° = 0.12°, and φ = 57.7°. By performing similar calculations and by using the data presented in Fig. 5c and 5d for the 2-NLG sample, we obtained α_{0° = 0°, α_{90° = 0.82°, and φ = 0°. Therefore, in the case of root-like MBLs, the disorientation of the crystal lattice of the InGaAs layer was mainly affected by the inclination of the layer relative to plane (001). What is more, there was no torsion of the lattice, which can also be indirectly confirmed by scanning at coordinates ω–φ. According to [17], large values of angles α correlate with low efficiency of elastic strain relaxation in the structure through the formation of dislocations. Therefore, the disorientation of the crystal lattice is a secondary mechanism for relieving residual strain. In the case of the 2-NLG sample, this may mean that during the early stages of the buffer layer growth, the strain relaxation mechanism was mainly due to the formation of dislocations, while further it was a tilt of the lattice that was responsible for the release of excessive strain.

4. Conclusions

In our study, for the growth of active layers of $In_{0.83}Ga(Al)_{0.17}As$ on InP substrates, we proposed two alternative designs of the metamorphic buffer layer: one following a linear law of the composition variation and the other following a nonlinear law, which in the studied case had a square root-like dependence. To determine the effectiveness of these metamorphic buffer layers, we used transmission electron microscopy and the reciprocal space mapping of X-ray diffraction intensity to study the crystalline quality of the bulk $In_{0.83}Ga(Al)_{0.17}As$ layers grown on the buffer layers. The reciprocal space mapping for asymmetric reflections from a set of planes (224) showed that the active layers were partially strain-free in heterostructures with both linear and nonlinear buffer layer. They also revealed the formation of misfit dislocations. The reciprocal space mapping in the geometry of symmetrical reflections (004) allowed establishing that in both samples elastic strain was relieved through the disorientation of the crystal lattice relative to the plane of the substrate. The density of threading dislocations in the active layers of $In_{0.83}Ga(Al)_{0.17}As$ in the heterostructure with a linear metamorphic buffer layer calculated from the images of transmission electron microscopy was ~ $5 \cdot 10^8$ cm^{-2}. Presumably, in order to reduce it and to obtain a dislocation-free region in the heterostructure, the growth of the linear metamorphic buffer layer must be completed with an inverse step with an increase in the mole fraction of indium in the composition of the buffer layer relative to the composition of the active layers.

Contribution of the authors

The authors contributed equally to this article.

Conflict of interests

The authors declare that they have no known competing financial interests or personal relationships that could have influenced the work reported in this paper.

References

1. Galiev G. B., Vasil'evskii I. S., Pushkarev S. S., ... Dwir E. I. Suvorova metamorphic InAlAs/InGaAs/InAlAs/GaAs HEMT heterostructures containing strained superlattices and inverse steps in the metamorphic buffer. *Journal of Crystal Growth*. 2013;366: 55–60. https://doi.org/10.1016/j.jcrysgro.2012.12.017

2. Kettler T., Karachinsky L. Ya., Fiol G., ... Ledentsov N. N. Degradation-robust single mode continuous wave operation of 1.46 μm metamorphic quantum dot lasers on GaAs substrate. *Applied Physics Letters*. 2006;89(4): 041113. https://doi.org/10.1063/1.2236291

3. Egorov A. Yu., Karachinsky L. Ya., Novikov I. I., Babichev A. V., Nevedomskiy V. N., Bugrov V. E. Optical properties of metamorphic GaAs/InAlGaAs/InGaAs heterostructures with InAs/InGaAs quantum wells, emitting light in the 1250–1400 nm spectral range. *Semiconductors*. 2016;50(5): 612–615. https://doi.org/10.1134/S1063782616050079

4. Egorov A. Yu., Karachinsky L. Ya., Novikov I. I., Babichev A. V., Berezovskaya T. N., Nevedomskiy V. N. Metamorphic distributed Bragg reflectors for the 1440–1600 nm spectral range: epitaxy, formation, and regrowth of mesa structures. *Semiconductors*. 2015;49(10): 1388–1392. https://doi.org/10.1134/S1063782615100073

5. Garcia I., France R. M., Geisz J. F., McMahon W. E., Steiner M. A., Johnston S., Friedman D. J. Metamorphic III–V solar cells: recent progress and potential. *IEEE Journal of Photovoltaics*. 2015;6(1): 366–373. https://doi.org/10.1109/JPHOTOV.2015.2501722

6. Liu Y., Ma Y., Li X., ... Gong H. High temperature behaviors of 1–2.5 μm extended wavelength $In_{0.83}Ga_{0.17}As$ photodetectors on InP substrate. *IEEE Journal of Quantum Electronics*. 2021;57(4): 1–7. https://doi.org/10.1109/JQE.2021.3087324

7. Gendry M., Drouot V., Santinelli C., Hollinger G. Critical thicknesses of highly strained InGaAs layers grown on InP by molecular beam epitaxy. *Applied Physics Letters*. 1992;60(18): 2249–2251. https://doi.org/10.1063/1.107045

8. Ji X., Liu B., Tang H., ... Yan F. 2.6 μm MBE grown InGaAs detectors with dark current of SRH and TAT. *AIP Advances*, 2014;4(8): 087135. https://doi.org/10.*1063*/1.4894142

9. Vasilkova E. I., Pirogov E. V., Sobolev M. S., Ubiyvovk E. V., Mizerov A. M., Seredin P. V. Molecular beam epitaxy of metamorphic buffer for InGaAs/InP photodetectors with high photosensitivity in the range of 2.2–2.6 um. *Condensed Matter and Interphases*. 2023;25(1): 20–26. https://doi.org/10.17308/kcmf.2023.25/10972

10. Pobat D. B., Solov'ev V. A., Chernov M. Yu., Ivanov S. V. Distribution of misfit dislocations and elastic mechanical stresses in metamorphic buffer InAlAs layers of various constructions. *Physics of the Solid State*. 2021;63(1): 84–89. https://doi.org/10.1134/s1063783421010170

11. Solov'ev V. A., Chernov M. Yu., Sitnikova A. A., Brunkov P. N., Meltser B. Ya., Ivanov S. V. Optimization of the structural properties and surface morphology of a convex-graded $In_xAl_{1-x}As$ (x = 0.05–0.83) metamorphic buffer layer grown via MBE on GaAs (001). *Semiconductors*. 2018;52(1): 120–125. https://doi.org/10.1134/s1063782618010232

12. Chen X., Gu Y., Zhang Y. Epitaxy and device properties of InGaAs photodetectors with relatively high lattice mismatch. *Epitaxy*. 2018: 203. https://doi.org/10.5772/intechopen.70259

13. Fewster P. F. Reciprocal space mapping. *Critical Reviews in Solid State and Material Sciences*. 1997;22(2): 69–110. https://doi.org/10.1080/10408439708241259

14. Bellani V., Bocchi C., Ciabattoni T., ... Trevisi G. Residual strain measurements in InGaAs metamorphic buffer layers on GaAs. *The European Physical Journal B*. 2007;56: 217–222. https://doi.org/10.1140/epjb/e2007-00105-8

15. Fewster P. F. X-ray diffraction from low-dimensional structures. *Semiconductor Science and Technology*. 1993;8(11): 1915. https://doi.org/10.1088/0268-1242/8/11/001

16. Vasil'evskii I. S., Pushkarev S. S., Grekhov M. M., Vinichenko A. N., Lavrukhin D. V., Kolentsova O. S. Features of the diagnostics of metamorphic InAlAs/InGaAs/InAlAs nanoheterostructures by high-resolution X-ray diffraction in the ω-scanning mode. *Semiconductors*. 2016;50(4): 559–565. https://doi.org/10.1134/s1063782616040242

17. Lee D., Park M. S., Tang Z., Luo H., Beresford R., Wie C. R. Characterization of metamorphic $In_xGa_{1-x}As$/GaAs buffer layers using reciprocal space mapping. *Journal of Applied Physics*. 2007;101(6):063523, https://doi.org/10.1063/1.2711815

18. Aleshin A. N., Bugaev A. S., Ermakova M. A., Ruban O. A. Investigation of MHEMT heterostructure with In0.4Ga0.6As channel, grown by MBE on GaAs substrate, using reciprocal space mapping. *Semiconductors*. 2015;49(8):1065. Available at: https://journals.ioffe.ru/articles/viewPDF/42087

19. Chauveau J.-M., Androussi Y., Lefebvre A., Persio J. Di, Cordier Y. Indium content measurements in metamorphic high electron mobility transistor structures by combination of X-ray reciprocal space mapping and transmission electron microscopy. *Journal of Applied Physics*. 2003;93(7): 4219–4225. https://doi.org/10.1063/1.1544074

Information about the authors

Elena I. Vasilkova, postgraduate student, Engineer, Alferov University (Saint Petersburg, Russian Federation).
https://orcid.org/0000-0002-0349-7134
elenvasilkov@gmail.com

Evgeny V. Pirogov, Researcher, Alferov University (Saint Petersburg, Russian Federation).
https://orcid.org/0000-0001-7186-3768
zzzavr@gmail.com

Vladimir N. Nevedomskiy, Senior Researcher, Ioffe Physical-Technical Institute of the Russian Academy of Sciences (Saint Petersburg, Russian Federation).
https://orcid.org/0000-0002-7661-9155
vladimir.nevedomskiy@connector-optics.com

Oleg V. Barantsev, student, Lab Assistant, Alferov University (Saint Petersburg, Russian Federation).
https://orcid.org/0009-0001-6873-8488
ovbarantsev@gmail.com

Kirill O. Voropaev, Head of the Group, JSC "OKB-Planeta" (Velikiy Novgorod, Russian Federation).
https://orcid.org/0000-0002-6159-8902
kirill.voropaev@novsu.ru

Andrey A. Vasil'ev, Engineer-Technologist, JSC "OKB-Planeta" (Velikiy Novgorod, Russian Federation).
https://orcid.org/0009-0009-2615-6795
Wasiliew.andre@yandex.ru

Leonid Ya. Karachinsky, Dr. Sci. (Tech.), Chief Researcher, Alferov University and Leading Researcher, ITMO University (Saint Petersburg, Russian Federation).
https://orcid.org/0000-0002-5634-8183
karach@switch.ioffe.ru

Innokenty I. Novikov, Cand. Sci. (Phys.–Math.), Senior Researcher, Alferov University and Senior Researcher, ITMO University (Saint Petersburg, Russian Federation).
https://orcid.org/0000-0003-1983-0242
novikov@switch.ioffe.ru

Maxim S. Sobolev, Cand. Sci. (Phys.–Math.), Head of the Laboratory, Alferov University (Saint Petersburg, Russian Federation).
https://orcid.org/0000-0001-8629-2064
sobolevsms@gmail.com

Received 15.04.2024; approved after reviewing 30.04.2024; accepted for publication 06.05.2024; published online 25.03.2025.

Translation by Irina Charychanskaya